AMERICAN SOCIETY FOR MICROBIOLOGY | Applied and Environmental Microbiology

Environmental Microbiology | Full-Length Text

Semi-rational design of nitroarene dioxygenase for catalytic ability toward 2,4-dichloronitrobenzene

Jia Xu,[1] **Tao Li,**[1] **Wei E. Huang,**[2] **Ning-Yi Zhou**[1]

AUTHOR AFFILIATIONS See affiliation list on p. 14.

ABSTRACT Rieske non-heme dioxygenase family enzymes play an important role in the aerobic biodegradation of nitroaromatic pollutants, but no active dioxygenases are available in nature for initial reactions in the degradation of many refractory pollutants like 2,4-dichloronitrobenzene (24DCNB). Here, we report the engineering of hotspots in 2,3-dichloronitrobenzene dioxygenase from *Diaphorobacter* sp. strain JS3051, achieved through molecular dynamic simulation analysis and site-directed mutagenesis, with the aim of enhancing its catalytic activity toward 24DCNB. The computationally predicted activity scores were largely consistent with the detected activities in wet experiments. Among them, the two most beneficial mutations (E204M and M248I) were obtained, and the combined mutant reached up to a 62-fold increase in activity toward 24DCNB, generating a single product, 3,5-dichlorocatechol, which is a naturally occurring compound. *In silico* analysis confirmed that residue 204 affected the substrate preference for *meta*-substituted nitroarenes, while residue 248 may influence substrate preference by interaction with residue 295. Overall, this study provides a framework for manipulating nitroarene dioxygenases using computational methods to address various nitroarene contamination problems.

IMPORTANCE As a result of human activities, various nitroaromatic pollutants continue to enter the biosphere with poor degradability, and dioxygenation is an important kickoff step to remove toxic nitro-groups and convert them into degradable products. The biodegradation of many nitroarenes has been reported over the decades; however, many others still lack corresponding enzymes to initiate their degradation. Although rieske non-heme dioxygenase family enzymes play extraordinarily important roles in the aerobic biodegradation of various nitroaromatic pollutants, prediction of their substrate specificity is difficult. This work greatly improved the catalytic activity of dioxygenase against 2,4-dichloronitrobenzene by computer-aided semi-rational design, paving a new way for the evolution strategy of nitroarene dioxygenase. This study highlights the potential for using enzyme structure-function information with computational pre-screening methods to rapidly tailor the catalytic functions of enzymes toward poorly biodegradable contaminants.

KEYWORDS biodegradation, molecular dynamics simulation, nitroarene dioxygenase, semi-rational design, site-directed mutagenesis

Hundreds of synthetic nitroarenes are globally produced and used as chemical feedstocks for the manufacturing of drugs, dyes, pesticides, and explosives (1). However, contaminants of various nitroarenes have been released into the biosphere from industrial wastes or improper handling of chemical products (2). These compounds are more toxic than their parent aromatic compounds and are resistant to biodegradation due to the presence of electron-withdrawing nitro groups (sometimes halogen groups) (3, 4). Exposure to nitroarenes may cause the formation of DNA adducts, which

Editor Martha Vives, Universidad de los Andes, Bogotá, Colombia

Address correspondence to Ning-Yi Zhou, ningyi.zhou@sjtu.edu.cn, or Wei E. Huang, wei.huang@eng.ox.ac.uk.

Jia Xu and Tao Li contributed equally to this article. Author order was determined by drawing straws.

The authors declare no conflict of interest.

See the funding table on p. 14.

Received 21 August 2023
Accepted 5 April 2024
Published 6 May 2024

further lead to carcinogenesis, mutagenesis, and teratogenesis (2). Therefore, a number of nitroarenes have been listed as priority pollutants by the United States Environmental Protection Agency (5).

The prior treatment for nitroarenes in the environment would be an effective biodegradation that eliminates its poisonous nitro group. The potential of microorganisms to degrade recalcitrant nitroarenes has been invoked by the characterization of bacteria capable of growing on nitroaromatic substrates, for example, 2-nitrotoluene (2NT) (6), nitrobenzene (7), 3-nitrotoluene (3NT) (8), 2,4-dinitrotoluene (24DNT) (9, 10), 2-chloronitrobenzene (2CNB) (11), and 2,3- and 3,4-dichloronitrobenzene (DCNB) (12). Rieske non-heme iron dioxygenases are versatile enzymes that play an important role in xenobiotic degradation; notably, they kick-start the nitroarenes' degradation pathway with the formation of the biodegradable catechols and the release of nitrite (1). This type of enzymes contains three components, namely ferredoxin reductase, Rieske ferredoxin, and $\alpha_3\beta_3$ terminal oxygenase. Each α subunit of oxygenase contains a Rieske [2Fe–2S] cluster and a mononuclear iron (II) catalytic center, which is related to electron transfer and substrate oxidation, respectively (13, 14). Generally, nitroarene dioxygenases share ≥80% amino acid sequence identity (Fig. 1A), and some key residues from the catalytic domain of the α subunit contribute to the difference in their substrate specificity (3, 15–18).

Extensive research has been conducted on several nitroarene dioxygenases, including crystal structure data (20, 21), computational chemical studies (22–26), peroxide shunt (27), and substrate turnover (28, 29) experiments. Therefore, the catalytic site and substrate binding site at the active center in α subunits of oxygenase and the substrate oxidation mechanism are gradually uncovered and become clear. Nitroarene dioxygenases in general share a similar substrate binding mode, with the right exposure of their susceptible sites for the electrophilic attack to the iron center. The entry of substrate into the active site leads to the rearrangement of water molecules and ligands to form Fe^{III}-(hydro)peroxo species ($[Fe_{III}–OOH]^{2+}$), and a dioxygenation attack is initiated through the generation of a peroxo-bridged substrate radical between the substrate and Fe-oxygen species (25–29). In this process, a good substrate fit in the active site is a prerequisite for O_2 activation. Some nitroarene dioxygenases possess an asparagine at position 258, which will form a hydrogen bond (H-bond) between its amino group and the nitro group of the substrate (14–16, 21). This interaction is believed to play an extremely important role in the proper positioning and stable binding of nitroarene substrates.

However, in spite of decades of efforts made in isolating nitroarene degraders and identifying enzymes involved, many nitroarene pollutants have remained poorly biodegradable. Take 2,4-dichloronitrobenzene (24DCNB) as an example, which is a high-production volume chemical (greater than one million pounds per year) (30) used for the synthesis of 2,4-difluoroaniline and detected in multifarious industrial wastewater (31–33). Compared to its isomers 23DCNB or 3,4-dichloronitrobenzene (34DCNB), 24DCNB is not only genotoxic but also considered to be a possible human carcinogen (34–36). The large quantity of usage, refractoriness, genotoxicity, carcinogenicity, and toxicity of 24DCNB have prompted researchers to search for efficient and economical environmental remediation approaches (31–33, 37, 38). Various bio-electrochemical methods have been proposed to remove 24DCNB from wastewater (31–33, 37, 38); however, no strains or enzymes have been reported to be capable of degrading 24DCNB yet.

Computer-aided directed evolution of proteins has been proven to have the superior capability of modifying proteins for desired functions (39, 40). Especially for those enzymes that lack a high-throughput screening method, rational design based on information on protein structure and mutagenesis hotspots and the support of computational tools offer an effective solution, which creates a significantly smaller variant library and provides *in silico* prescreening (41). Recently developed tools, including computer-based prediction of protein structures (42, 43), molecular docking (44, 45), and molecular dynamic (MD) simulation (46, 47), would dramatically bridge the gap between limited enzyme resources and explosive growth of artificial chemical compounds.

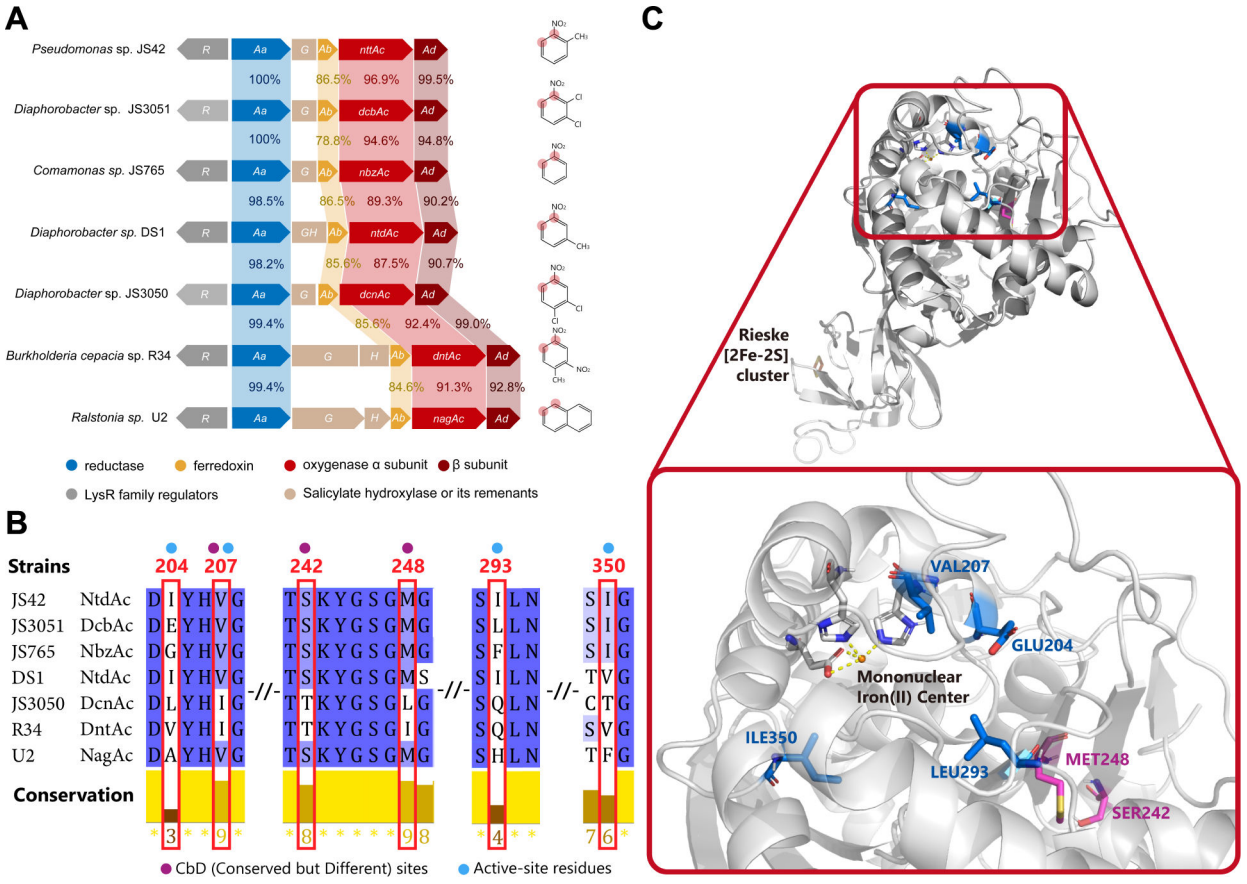

FIG 1 23DCNB dioxygenase mutant library design. (A) Comparison of various Nag-like dioxygenase gene clusters, arranged in order of pairwise identity. The corresponding substrates are presented on the right, with their attack sites of dioxygenation marked in red shades. (B) Sequence alignment of the α subunit of various Nag-like dioxygenases. The degree of conservation was calculated by Jalview (19), shown from low (white) to high (blue) as well. Six chosen sites are highlighted by frames in red. Chosen reasons are given above the sites in the form of small circles in corresponding colors. (C) Chosen residues for mutation marked in the homologous model of α subunit of 23DCNB dioxygenase.

Herein, we applied an *in silico* method to expedite the improvement of the catalytic activity of nitroarene dioxygenase toward 24DCNB. Through computationally predicting and experimentally verifying catalytic activity, two advantageous mutations (E204M and M248I) were selected from a small mutant library containing 14 single-site mutants of 23DCNB dioxygenase, and after combining these two advantageous mutations together, E204M-M248I showed a 62-fold increase in activity toward 24DCNB. The computer-assisted methodology employed in this study provides a framework for enhancing the activity of nitroarene dioxygenases toward recalcitrant nitroarenes.

MATERIALS AND METHODS

Chemicals, plasmids, bacterial strains, and culture conditions

2-nitrotoluene, 4-nitrotoluene, 1-nitronaphthalene, 2,5-dichloronitrobenzene, 2,4-dinitrotoluene, 2,6-dinitrotoluene, 3-methylcatechol, 4-methylcatechol, 3-chlorocatechol, 4-chlorocatechol, 3,4-dichlorocatechol, 3,5-dichlorocatechol, 4,5-dichlorocatechol, and 4-methyl-5-nitrocatechol were purchased from Sigma-Aldrich (USA), and their purity is >99%. 2-chloronitrobenzene (>99%), 3-chloronitrobenzene (>99%), 4-chloronitrobenzene (>99.5%), and 2-chloro-3-nitrotoluene (>98%) were purchased from Aladdin (China). 3-nitrotoluene (>99%) and 2,4-dichloronitrobenzene (>99%) were purchased from TCL (China). 4-chloro-3-nitrotoluene (99.36%) and 3,5-dichloronitrobenzene (98%)

were purchased from Bidepharm (China). 6-chloro-2-nitrotoluene (99%) and 2,3-dichloronitrobenzene (99%) were purchased from Macklin (China). In addition, 3,4-dichloronitrobenzene (99%) was purchased from Alfa Aesar (China) and 2,4-dinitrochlorobenzene (99%) from Adamas-beta (China). The plasmid pETDuet-DCB harboring the genes for 23DCNB dioxygenase was constructed previously (48) by inserting the *dcbAaAb* fragment between *Nco*I and *Sac*I, and the *dcbAcAd* fragment between *Nde*I and *Kpn*I. *Escherichia coli* DH5α and *Escherichia coli* BL21(DE3) were used for cloning and expressing mutant proteins, respectively. *E. coli* strains were cultured at 37°C in lysogeny broth (LB) or LB agar with appropriate antibiotics.

Site-directed mutagenesis

Site-directed mutagenesis of *dcbAc* was performed as the method described previously (48). Briefly, plasmid pETDuet-DCB, which was used as the template, was amplified by Phanta Max Super-Fidelity DNA Polymerase (Vazyme Biotech Co., Ltd, China) with complementary mutagenic primers described in Table 1. Then, the PCR products were digested using *Dpn*I, and the resulting products were transformed in the host bacteria into *E. coli* DH5α and screened on LB agar with 100 µg/mL ampicillin.

Whole-cell biotransformation assays to determine the specific activity of dioxygenase mutants

E. coli BL21 (DE3) (pETDuet-DCB) cells were grown in LB medium at 37°C until the optical density at 600 nm ($OD_{600\ nm}$) reached 0.8, which was measured in a BioTek EPOCH 2 microplate reader. Then, 0.1 mM isopropyl-β-D-thiogalactopyranoside (IPTG) was added

TABLE 1 Mutagenic primers used in this study

Primer	Sequence
E204F-F	5′-GCTGAAAACTTCGTTGGTGACTTCTACCACGTTGGTTGGACCCAC-3′
E204F-R	5′-GTGGGTCCAACCAACGTGGTAGAAGTCACCAACGAAGTTTTCAGC-3′
E204I-F	5′-TGAAAACTTCGTTGGTGACATATACCACGTTGGTTGGACC-3′
E204I-R	5′-GGTCCAACCAACGTGGTATATGTCACCAACGAAGTTTTCA-3′
E204L-F	5′-GGTCCAACCAACGTGGTATATGTCACCAACGAAGTTTTCA-3′
E204L-R	5′-GGTCCAACCAACGTGGTATAAGTCACCAACGAAGTTTTCA-3′
E204M-F	5′-GCTGAAAACTTCGTTGGTGACATGTACCACGTTGGTTGGACCCAC-3′
E204M-R	5′-GTGGGTCCAACCAACGTGGTACATGTCACCAACGAAGTTTTCAGC-3′
E204W-F	5′-GCTGAAAACTTCGTTGGTGACTGGTACCACGTTGGTTGGACCCAC-3′
E204W-R	5′-GTGGGTCCAACCAACGTGGTACCAGTCACCAACGAAGTTTTCAGC-3′
E204Y-F	5′-GTGGGTCCAACCAACGTGGTACCAGTCACCAACGAAGTTTTCAGC-3′
E204Y-R	5′-GTGGGTCCAACCAACGTGGTACCAGTCACCAACGAAGTTTTCAGC-3′
V207I-F	5′-GGTGACGAATACCACATTGGTTGGACCCACG-3′
V207I-R	5′-CGTGGGTCCAACCAATGTGGTATTCGTCACC-3′
S242T-F	5′-CTGGTCTGCAGATGACCACTAAATACGGTTCTGGT-3′
S242T-R	5′-ACCAGAACCGTATTTAGTGGTCATCTGCAGACCAG-3′
M248I-F	5′-ACCTCTAAATACGGTTCTGGTATAGGTCTGACCTGG-3′
M248I-R	5′-CCAGGTCAGACCTATACCAGAACCGTATTTAGAGGT-3′
L293H-F	5′-GCTCGTATCTACCGTTCTCATCTGAACGGTACTGTTTTCC-3′
L293H-R	5′-GGAAAACAGTACCGTTCAGATGAGAACGGTAGATACGAGC-3′
L293I-F	5′-TGCTCGTATCTACCGTTCTATACTGAACGGTACTGTTTTCC-3′
L293I-R	5′-GGAAAACAGTACCGTTCAGTATAGAACGGTAGATACGAGCA-3′
L293Q-F	5′-TCGTATCTACCGTTCTCAGCTGAACGGTACTGTTT-3′
L293Q-R	5′-AAACAGTACCGTTCAGCTGAGAACGGTAGATACGA-3′
I350T-F	5′-CGCTGTTCAGCGTTCTACCGGTCCGGC-3′
I350T-R	5′-GCCGGACCGGTAGAACGCTGAACAGCG-3′
I350V-F	5′-TGACGCTGTTCAGCGTTCTGTCGGTCCGGC-3′
I350V-R	5′-GCCGGACCGACAGAACGCTGAACAGCGTCA-3′

before incubating overnight at 16°C to induce dioxygenase expression. The cells were harvested, washed twice with phosphate-buffered saline (PBS), and suspended with PBS containing 80–200 µM 24DCNB. Specific activities were determined by measuring the rate of nitrite formed at appropriate intervals (depending on the activity of each mutant) during exposure to 200 µM 24DCNB or 23DCNB with shaking (220 rpm, 30°C). Nitrite was detected by the Griess method as described previously (49). To measure the protein concentration, cell pellets were recollected by centrifugation, suspended in equal volumes of 0.1 M NaOH, and boiled for 10 min. After that, protein concentration was measured by the Bradford method (50) with bovine serum albumin as the standard. Concentrations of 24DCNB and 3,5-dichlorocatechol (35DCC) were quantified by high-performance liquid chromatography (HPLC). To determine the protein expression pattern, 1 mL of cell cultures was harvested and resuspended with equal volumes of sodium dodecyl sulfate-polyacrylamide gel (SDS-PAGE) running buffer. Samples (20 mL each) were analyzed by 12% SDS-PAGE.

Analytical methods

Reverse-phase HPLC with a Waters e2695 separation module equipped with a Waters 2998 photodiode array detector and a C_{18} reversed-phase column (5 mm, 4.6 × 250 mm) at 30°C was used to quantify the compound concentrations of 24DCNB and 35DCC. The mobile phase consisted of water containing 0.1% (vol/vol) acetic acid (A) and methanol (B), eluted with 20% of solvent B for 5 min and linearly increased to 90% B after 30 min.

The products of biotransformation were identified by gas chromatography-mass spectrometry (GC-MS), which was performed with a TSQ 8000 Evo Triple Quadrupole GC-MS/MS (Thermo Fisher Scientific Inc., MA, USA) equipped with a capillary column HP-5MS (0.25 mm ×30 m, Agilent Technologies, CA, USA). For GC-MS analysis, biotransformation samples were extracted with an equal volume of ethyl acetate, which was then evaporated to dryness and dissolved in 0.2 mL of ethyl acetate. Samples were further derivatized by adding equal volumes of *N, O*-bis(trimethylsilyl)trifluoroacetamide at 70°C for 30 min. GC/MS program setting: the inlet temperature was set at 280°C, and the initial temperature was 70°C for 2 min, raised to 130°C at 5°C/min, increased to 180°C at 10°C/min, increased to 285°C at 5°C/min, and held for 5 min. Mass spectrometer conditions: 33–750 *m/z* mass range at the electron energy of 70 eV, EI energy source.

Simulation system preparation

The initial structure of mutated α subunits of dioxygenases was generated by AlphaFold2 (43), and all models were obtained with a high confidence level [an average plDDT (confidence) of 97]. The protonation states of protein residues were verified, and their hydrogen atoms were added by using H++ web server (51). The enzyme-ligand complex was assumed to be in its transition state, with Fe^{III}-(hydro)peroxo species formed in the active site. Therefore, a hydro(peroxo) moiety was placed next to the central iron by following the method reported previously (14), and the ligand (24DCNB) was docked to the predicted models with AutoDock Vina (44). Then, the program MCPB (52, 53) was used to generate force field parameters for $[Fe_{III}–OOH]^{2+}$ and Rieske [2Fe–2S] cluster using the ff99SB force field, while the Gaussian 16 (54, 55) was used to calculate the optimized geometries, force constants, and ESP charges. The resultant amber topology was further transformed into a GROMACS topology using ACPYPE (56).

Molecular dynamic simulation

The MD simulations were performed using the GROMACS 2020 (57) with the ff99SB force field. TIP3P-type water molecules and counter ions were filled into an extended 1 nm cubic box to generate a neutralized system, and the temperature and pressure of the simulation system were set at 300 K and 1 bar separately. The prepared system first went through 50,000 steps of steepest descent minimization until the maximum force <5.0 kJ/mol, followed by 100 ps of equilibration using NVT and NPT simulations, respectively.

During these two simulation phases, the protein and ligand were held fixed by using position restraints with a force constant of 1,000 kJ mol^{-1} nm^{-2}. The V-rescale method was used for the maintenance of constant temperature and the Parrinello-Rahman method for constant pressure. LINCS algorithm (58) was used to constrain all covalent bonds involving hydrogen atoms. The particle mesh Ewald method (59) with a grid length of 0.16 Å was used to calculate the electrostatic interactions. For each system, a 20 ns of MD simulation was carried out under the same conditions and repeated three times with a different random number, and some selected ones were extended to 200 ns.

After obtaining the trajectory of the MD simulation, root mean square deviation (RMSD), root-mean-square fluctuation (RMSF), the distance and angle between atoms, and conformational clustering analysis were calculated using the *gmx rms, gmx rmsf, gmx distance, gmx gangle,* and *gmx cluster* commands. The resulting structures were visualized by PyMOL (60). POVME 3.0 (61) was used to measure the substrate pocket volume distribution of conformations captured every 5 ns beginning from the 100 ns trajectory. A dynamical cross-correlation matrix (DCCM) was obtained by using a Python script to calculate the correlation coefficients of the wild-type MD simulation every 50 ps in the last 10 ns trajectory.

RESULTS

Analysis of key residues and construction of the mutant library of 23DCNB dioxygenase

Considering the facts that the α subunits of Nag-like nitroarene dioxygenases exhibit high sequence conservation and determine the substrate specificity (3, 15–18), the differential residues of the α subunits are thus considered as potential hotspots for protein engineering (Fig. 1B). In terms of the structural resemblance of 23DCNB to our intended substrate 24DCNB, we chose the 23DCNB dioxygenase from *Diaphorobacter* sp. strain JS3051 (12, 48) as the starting enzyme to carry out further modifications. We focused on the residues around the active center that were loosely conserved or those conserved but at different sites (62) (Fig. 1B and C), especially the sites that may have an effect on substrate specificity mentioned in previous reports (3, 15–18, 48).

To enhance the dioxygenase's activity toward 24DCNB, a *para*-substituted nitroarene, residues VAL207, SER242, and MET248, predicted to affect the accommodation of the enzyme toward the *para*-substituted group, were mutated into the corresponding residues in 24DNT dioxygenase or 34DCNB dioxygenase. Residue 204, serving as a "gatekeeper," occupies a pivotal position, bridging the enzyme tunnel and binding pocket and controlling access to the active center (48, 63). While most Nag-like dioxygenases feature a hydrophobic amino acid at this position, the 23DCNB dioxygenase has a glutamic acid, which is believed to form a halogen bond with the C3 chlorine atom of 23DCNB (48). However, for our target substrate, 24DCNB, GLU at position 204 might disrupt proper substrate positioning. Hence, we substituted GLU204 with other hydrophobic amino acids featuring bulky side chains (ILE, LEU, MET, PHE, TRP, and TYR) to better shape the active center or enzyme tunnel. The remaining two selected hotspots were modified with amino acids from other characterized dioxygenases. In the end, a total of 14 mutations (E204F, E204I, E204L, E204M, E204Y, E204W, V207I, S242T, M248I, L293H, L293I, L293Q, I350T, and I350V) were generated. Three-dimensional structures of these variants, along with the wild-type 23DCNB dioxygenase, were predicted using AlphaFold2 (43) for further computational analysis.

In silico prediction and *in vivo* assessment of enzyme activity on 24DCNB

To roughly investigate the effect of six different residues on dioxygenase-24DCNB interactions and pre-screen the mutant library by catalytic potential, we carried out three times of 20-ns MD simulations for 14 mutants and wild type, all with 24DCNB docked at the active center of each α subunit. The RMSD values of all systems reached a plateau after the first 5-ns simulations (Fig. S1), indicating that most systems reached their equilibrium. Therefore, all data were observed and collected from 5 to 20 ns.

According to the catalytic process of nitroarene dioxygenases (14–16, 21, 25–29), the nitroarene substrate can be anchored through an H-bond interaction, facilitating subsequent electrophilic attack on its benzene ring and denitration. A stable H-bond between the amino group of Asn258 and the nitro group of the substrate ensures a stable conformation and correct position of 24DCNB with respect to center $[Fe_{III}–OOH]^{2+}$, which is an essential precondition for reaching the pre-reaction state. The probability of H-bond formation was assessed using two key parameters: (i) the Oa-Nd (d) distance, which represents the distance between the oxygen atom (acceptor) of the nitro group in 24DCNB and the nitrogen atom (donor) of Asn258, and (ii) the Nd-H···Oa angle (θ), which signifies the donor-hydrogen···acceptor angle (Fig. 2). In general, a hydrogen bond is considered proper when the acceptor-donor distance is around 3.0 Å and the donor-hydrogen···acceptor angle approaches 180° (64). The closer the hydrogen bond approaches these ideal geometric values, the stronger the bond becomes. Consequently, we established the geometric hydrogen bond criterion as d(Oa-Nd) ≤ 3.5 Å and θ (Nd-H···Oa) ≥ 150°. We then calculated the proportion of the frequency of the correct conformations to the total frequency within each 20-ns simulation system that meets this established criterion and recorded it as the probability of H-bond formation (HB-probability) (Fig. 3A).

On the other hand, a productive conformation should guarantee that C1 and C6 carbons of 24DCNB are the dihydroxylated positions, yielding the only possible product, 35DCC. Two parameters were used to evaluate productive and nonproductive conformations, characterized by O1-C1 (D_1) and O2-C6 (D_2) distances between the O1 and O2 oxygen of $[Fe_{III}–OOH]^{2+}$ and the C1 and C6 carbon of 24DCNB, respectively (Fig. 2). The average oxidation attack distances D_1 and D_2 were calculated and presented in Fig. 3B, all with a standard deviation between 0.03 and 0.07 nm. To allow a subsequent dioxygenated attack on the substrates, both distances must be appropriate.

In fact, the transiently equilibrated conformations and coordinates of 24DCNB in each 20-ns MD simulation system may not always accurately reflect their true state. The reliability of a docking conformation is directly proportional to its frequency, as the most frequently occurring one is more likely to be deemed trustworthy upon repetition. The majority of mutant dioxygenases and wild-type dioxygenase exhibited a low probability or no possibility of H-bond formation in most repetitions, with only five mutants generally showing high probability when repeated (Fig. 3A). Hence, these five mutants, namely E204I, E204L, E204M, E204Y, and M248I, were identified as being able to effectively establish H-bonds with the substrate 24DCNB.

On average, more than half of the populations successfully formed the H-bond in these five mutants' simulation systems. Specifically, E204M performed the best of all, with the highest HB-probability of 85.1% and an average probability of 62.7%.

The distribution of oxidation attack distance (Fig. 3B) exhibited a certain correlation with the distribution of HB-probability (Fig. 3A), owing to the relatively fixed positions of the iron center and Asn258. Specifically, when an H-bond was well-formed, 24DCNB tended to be anchored, thereby exposing the C1 and C6 carbon sites to the iron-oxygen complex; in other words, a high HB-probability often coincided with short oxidation attack distances. As demonstrated by the instances of E204I, E204L, E204M, and M248I, the mean distances of both D_1 and D_2 were roughly less than 0.4 nm. The distances between the oxygen atoms of the iron-oxygen complex and the reacting carbon atoms in the crystal structure of naphthalene dioxygenase (PDB ID: 1O7N) (20) are 0.32 and 0.28 nm, which is slightly smaller than the corresponding experimental values presented here. The conformation clustering analysis has confirmed that 24DCNB in the active site of these four mutants adopted a stable docking conformation throughout the 20-ns simulation (Fig. S2C), which is considered to have reached the pre-reaction state. However, E204Y is an exception, with a high probability of forming hydrogen bonds but relatively long distances for oxidation attacks. Different docking conformations were adopted during the 20-ns simulation of E204Y, with the C1 and C2 adjacent carbon atoms of 24DCNB being closest to the oxygen atom pair of $[Fe_{III}–OOH]^{2+}$ (Fig. S2A and

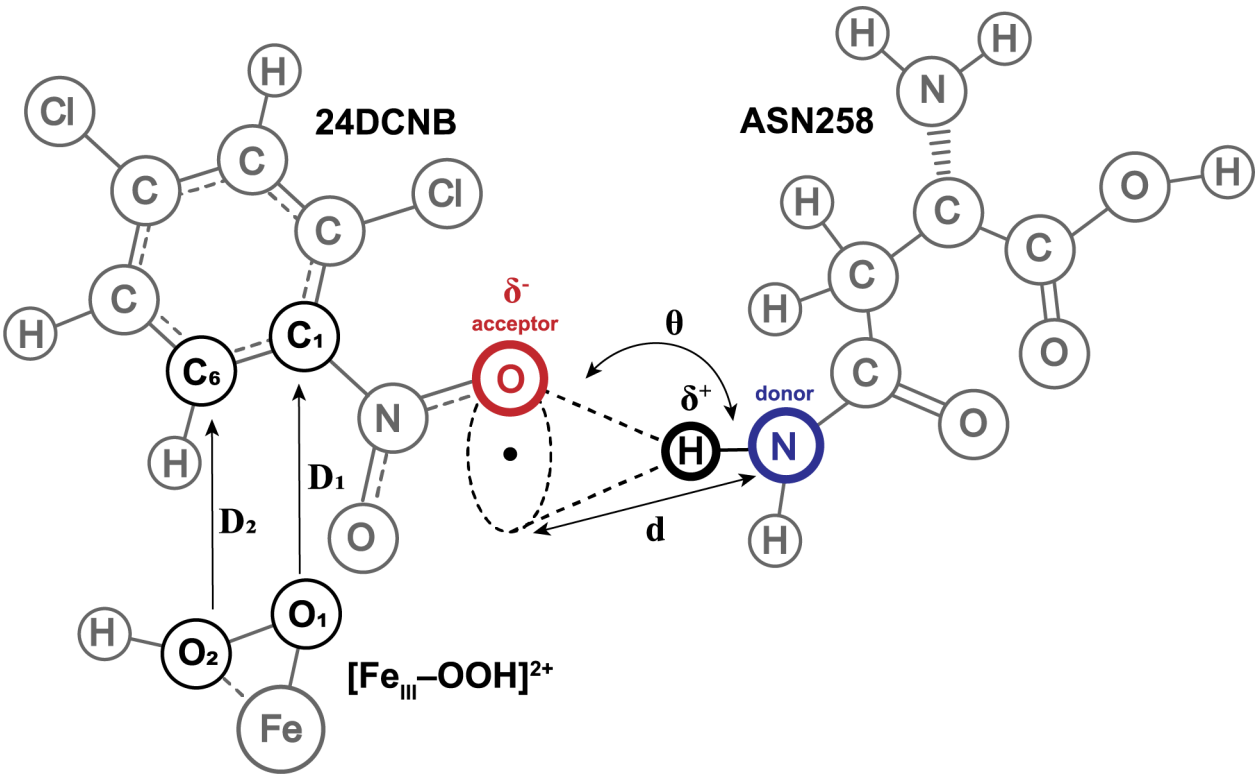

FIG 2 Parameters for the evaluation of H-bond formation probability and dioxygenation attack distance.

B). Despite this proximity, the presence of nitro and chlorine groups at these two sites hinders productive dioxygenation, as simultaneous denitration and dichlorination have not been observed thus far (3).

Considering both aspects that may reflect the catalytic potential of mutant dioxygenases toward 24DCNB, four mutants, E204I, E204L, E204M, and M248I, were supposed to be candidates for 24DCNB dioxygenase.

Meanwhile, to verify the actual dioxygenase activity, we conducted whole-cell biotransformation assays to obtain the specific enzyme activities of wild-type and 14 mutant dioxygenases toward 23DCNB and 24DCNB. Based on SDS-PAGE (Fig. S3), all of the mutations produced comparable amounts of dioxygenase proteins. As shown in Fig. 3C, except for L293I, the specific enzyme activity on the natural substrate 23DCNB was reduced to varying degrees in all mutants. More importantly, E204I, E204L, E204M, and M248I developed noticeable catalytical activity toward 24DCNB from nearly nothing, which is in agreement with the results of *in silico* prediction. It is interesting to note that three of them are mutations at residue 204, suggesting their importance in controlling substrate specificity and catalytic activity. When the glutamic acid at position 204 was mutated to methionine, the dioxygenase showed the highest activity toward both 23DCNB and 24DCNB among these three mutants.

Combination of beneficial mutations at sites 204 and 248

Epistasis describes a genetic phenomenon in which the combined effect of multiple mutations is not a simple addition of their individual effects but a more complex result, which also occurs in protein evolution (65). As mutations at residues 204 and 248 conferred the dioxygenase with a unique catalytic capacity, it is intriguing to explore the potential synergy of combining these two beneficial mutations and their impact on the enzyme's properties. Hence, a double mutant E204M-M248I was obtained. The *in vivo* specific activities of single-site and double-site mutants were determined with various nitroarene substrates (Fig. 4).

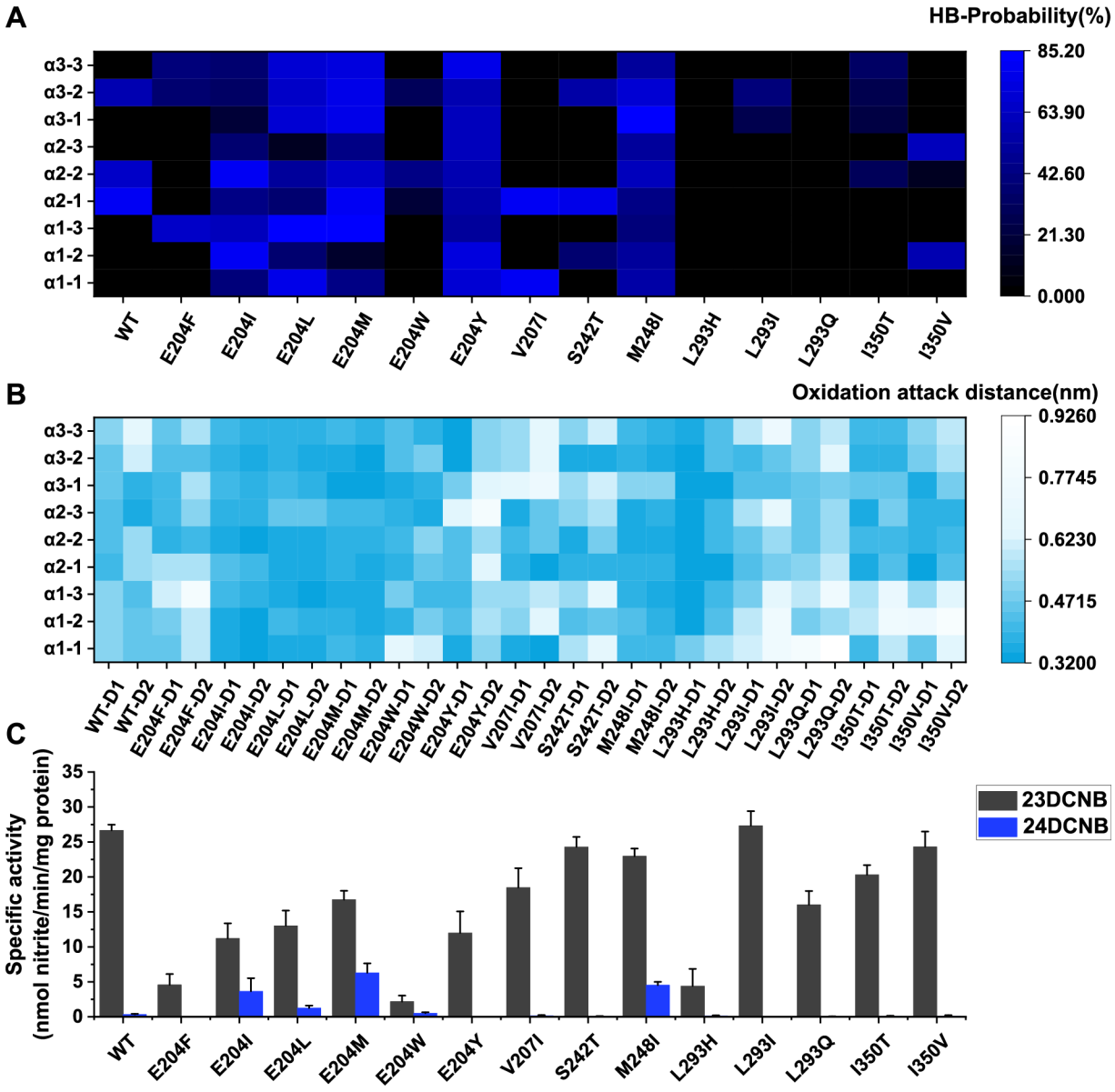

FIG 3 Predicted catalytic potential evaluated by H-bond formation probability (A), dioxygenation attack distance (B), and actual specific activity (C) of wild-type and mutant dioxygenases on 24DCNB. Each mutant has nine sets of data in panels A and B because there were three active sites in each $\alpha_3\beta_3$ system, which was repeated three times. The specific activity was obtained through whole-cell biotransformation assays with 23DCNB and 24DCNB as substrates. Values are data averages from at least three parallel experiments, and error bars are standard deviations.

Compared to wild-type dioxygenase, E204M mutation modulated the substrate preference of dioxygenase toward favoring *ortho*-substituted substrates more, significantly increasing the specific activity on 2NT and 2CNB by five- to ninefold, while having reduced activities on substrates with a *meta*-substituted group including 3NT, 3-chloronitrobenzene, 6-chloro-2-nitrotoluene, 2-chloro-3-nitrotoluene, 23DCNB, 34DCNB, 3,5-dichloronitrobenzene, 2,4-dinitrochlorobenzene (24DNCB), and 2,6-dinitrotoluene. The specific activity of the M248I mutant toward the majority of substrates tested was comparable to that of wild-type dioxygenase. But 34DCNB and 24DNCB, both have 3- and 4-substituted groups, saw a two- to fourfold increase in specific activity of M248I mutant compared with the wild type. After combining these two beneficial substitutions, the substrate specificity of dioxygenase was broadened notably. In particular, the E204M-M248I mutant greatly enhanced the activity toward substrates

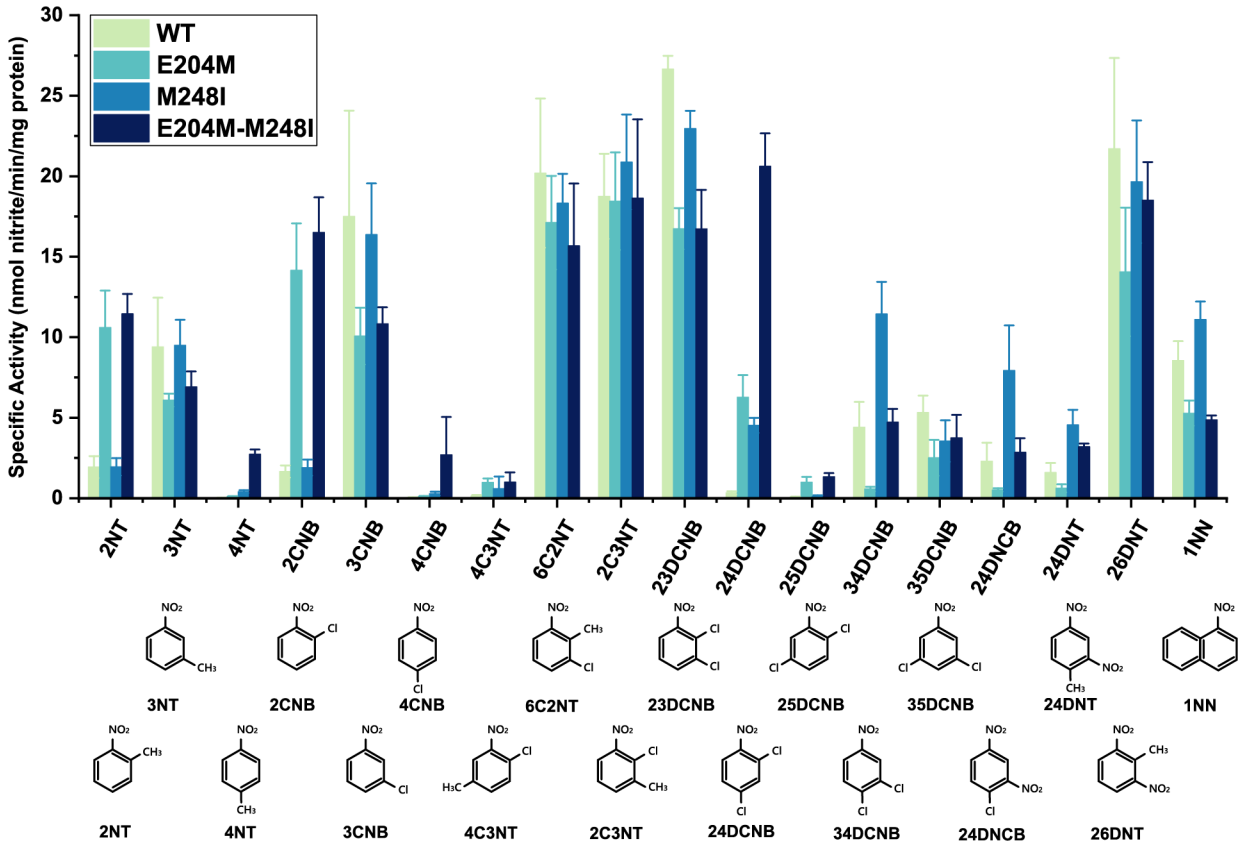

FIG 4 Substrate specificity of wild-type dioxygenase, E204M, M248I, and E204M-M248I mutants toward different nitroarenes. The specific activity was obtained through whole-cell biotransformation assays. Values are data averages from at least three parallel experiments, and error bars are standard deviations. 4NT, 4-nitrotoluene; 3CNB, 3-chloronitrobenzene; 4CNB, 4-chloronitrobenzene; 4C3NT, 4-chloro-3-nitrotoluene; 6C2NT, 6-chloro-2-nitrotoluene; 2C3NT, 2-chloro-3-nitrotoluene; 25DCNB, 2,5-dichloronitrobenzene; 35DCNB, 3,5-dichloronitrobenzene; 24DNCB, 2,4-dinitrochlorobenzene; 26DNT, 2,6-dinitrotoluene; and 1NN, 1-nitronaphthalene.

that have 2- or/and 4-substituted groups (2NT, 4NT, 2CNB, 4CNB, and 24DCNB). It is worth noting that E204M-M248I showed a 62-fold increase in specific activity on 24DCNB over the wild type. Such results indicate that E204M and M248I mutations exhibit positive epistasis, in which greater improvements in specificity and activity have been generated than expected.

Identification of biotransformation products by E204M-M248I

The course illustrating the biotransformation of 24DCNB to 35DCC catalyzed by E204M-M248I is presented in Fig. 5. Remarkably, E204M-M248I exhibited the ability to transform 24DCNB into 35DCC and nitrite in a stoichiometric 1:1:1 ratio. These results provide compelling evidence for a dioxygenation reaction targeting the C1 and C6 carbons of 24DCNB, thus validating the hypothesis previously proposed in our computer-aided prediction method.

Additionally, we performed characterization of the reaction products catalyzed by wild-type, E204M, M248I, and E204M-M248I mutants toward 18 distinct nitroaromatic substrates, as depicted in Fig. S5. Despite variable relative specific activities exhibited by different mutant dioxygenases toward various substrates (Fig. 4), the post-oxidation product composition of most substrates was largely consistent. All substrates except 4C3NT demonstrated susceptibility to oxidation at nitro-substituted positions on the aromatic ring, leading to the formation of catechol derivatives. Additionally, oxidation of certain substrates could also occur at methyl substituents, producing alcohol compounds, albeit without detectable dechlorination products.

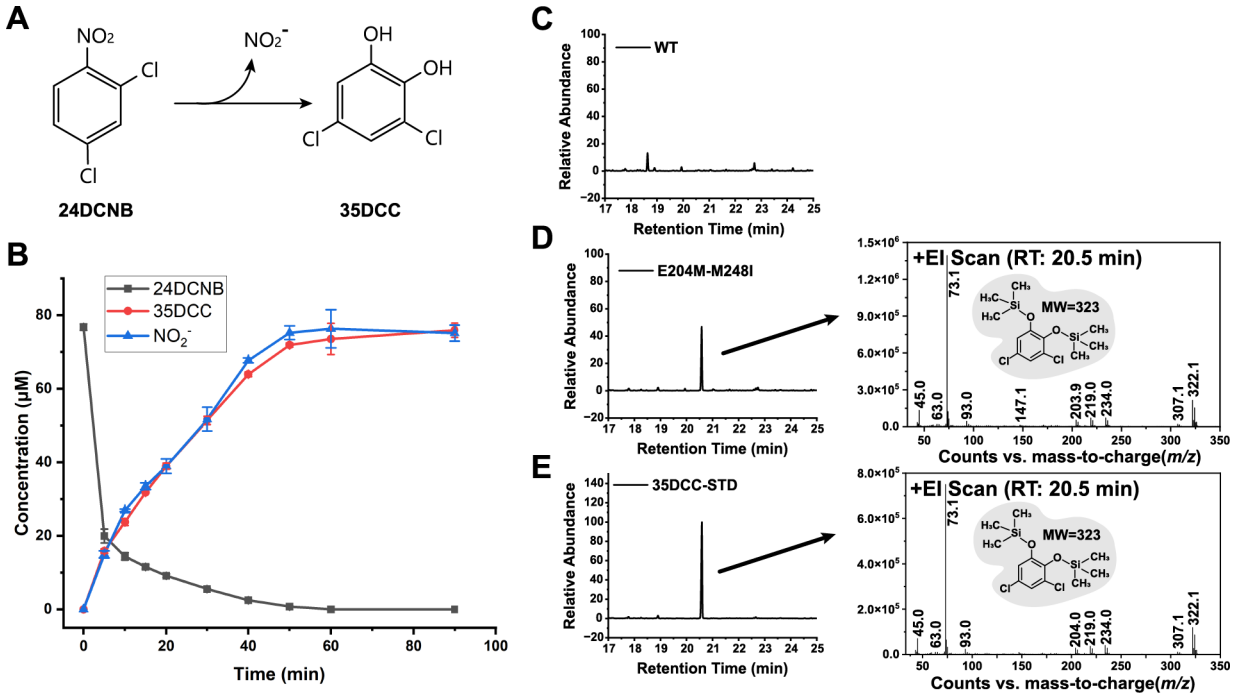

FIG 5 Whole-cell biotransformation of 24DCNB. (A) Reaction scheme of 24DCNB biotransformation. (B) Time course of 24DCNB conversion to 35DCC with nitrite release by IPTG-induced *E. coli* BL21(DE3) expressing E204M-M248I dioxygenase. The data shown are the averages of three technical duplicates of a typical experiment, and the outcomes of all separate trials were broadly consistent. Standard deviations are shown by error bars. (C–E) GC/MS total ion chromatogram. The product of 24DCNB biotransformation catalyzed by wild type (C) and E204M-M248I (D) was detected and compared with the authentic 35DCC (E). The mass spectra refer to 35DCC after derivatization.

In the case of substrate 2NT, the substitution of glutamate with methionine at position 204 resulted in an enhanced specificity for dioxygenation at the nitro group, yielding predominantly 3-methylcatechol as the primary product (66.3% and 77.2% for E204M and E204M-M248I, respectively). The M248I mutation impacts substrate specificity toward 34DCNB evidently, which shifts the dioxygenation site from positions 1 and 2 to positions 1 and 6, resulting in 90.7% of the generated products being 4,5-dichlorocatechol. The relative specific activity of the M248I mutant toward 34DCNB is also the highest compared to other mutants (Fig. 4). A significant alteration in substrate regiospecificity is observed with substrate 24DNT. E204M-M248I resulted in nearly all 24DNT being converted to 4-methyl-5-nitrocatechol, whereas the wild-type or single mutants converted less than half of the substrate to 4-methyl-5-nitrocatechol.

Further molecular dynamics analysis of E204M-M248I and two single-site mutants

Three times of 20-ns MD simulations of E204M-M248I and an additional 200-ns MD simulations separately for wild type, E204M, M248I, and E204M-M248I based on their 20-ns MD simulations were performed (Fig. S4), trying to shed light on the role of E204M and M248I mutations in influencing the enzyme properties. The H-bond formation and oxidation attack distances were also analyzed during the 5–200-ns simulation and presented in Fig. S6.

The substitution of glutamic acid at position 204 with methionine contributes to the hydrophobic environment in the binding site while maintaining a similar-sized sidechain. Given that residue 204 lies at the junction of the enzyme tunnel and binding pocket, a properly sized and hydrophobic sidechain can effectively shield the binding site from accessing the solvent and shape the binding pocket by steric hindrance. It is postulated that the mutation E204M could add compactness to the binding pocket so that the

24DCNB's spatial movement was much more constrained inside the pocket. It is reflected by decreased substrate pocket volume (Fig. 6) and decreased RMSFs of 24DCNB (Fig. 6). Furthermore, relative to the productive conformation of 24DCNB, the side chain of residue 204 is close to its C3 atom. A more compact active site chamber with narrowed space around the C3 atom of 24DCNB contributes to the improvement of catalytical activity of E204M mutant toward smaller *ortho*-substituted substrates like 2NT and 2CNB while leading to the weakening of activity toward *meta*-substituted substrates.

As for residue 248, its position is a certain distance away from the center iron at about 14 Å, and the orientation of its sidechain is in the opposite direction. Therefore, we applied DCCM to determine pairwise cross-correlation coefficients (C_{ij}) indicating the potential allosteric sites (66, 67). According to the computed DCCM of wild type (Fig. S7), the most obvious positive dynamic correlation was between M248 and N295 with a C_{ij} higher than 0.45, suggesting a potential epistatic effect between these two structural neighbors. Residue 295, as a well-conserved hydrophobic residue in Nag-like family dioxygenases (Fig. 1B), lies around the C4 atom of a properly docked 24DCNB and plays a critical part in maintaining and stabilizing the binding pocket. Mutation M248I thereby may make an impact on N295 and, in turn, affect the interactions between substrate and the binding pocket, as evidenced by the improved specific activity of M248I mutant toward substrates with 4-substituted groups. Besides, the M248I mutant has the largest substrate pocket volume among the wild-type, E204I, M248I, and E204I-M248I variants, providing larger binding space for bulky substrates like 1-NN, which is also in agreement with the experimental results (Fig. 4).

By combining two beneficial mutations, E204I-M248I has a higher possibility of H-bond formation, appropriate oxidation attack distances, and compact binding pocket (Fig. S6; Fig. 6). But it is unfortunate that such inconspicuous improvements obtained

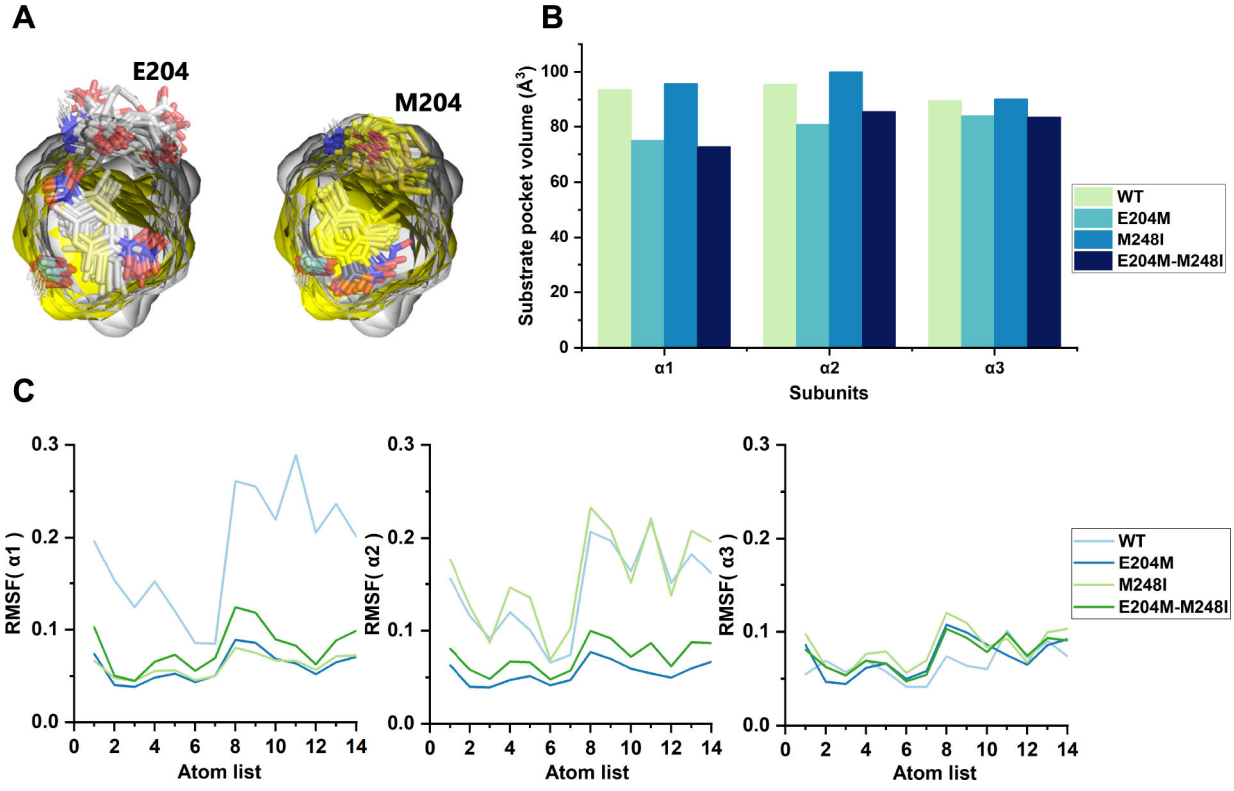

FIG 6 Pocket volume analysis and stability analysis of substrate docking. (A) The superposition of binding pockets of wild-type (gray) and E204M mutant (yellow) captured every 5 ns during 100–200-ns MD simulation trajectory (take α1 as an example). (B) The average pocket volume of each α subunit. (C) RMSF values of the 24DCNB in each α subunit.

from the MD simulation failed to explain the obvious synergistic epistasis between E204I and M248I observed in *in vivo*-specific activities.

DISCUSSION

The nitroarene dioxygenases from Gram-negative strains to date have all evolved from a common Nag-like naphthalene dioxygenase ancestor (10, 68–70). These dioxygenases possess a broad substrate spectrum but exhibit a greater preference for various nitro-aromatic compounds. The divergence in substrate specificity and regiospecificity of nitroarene dioxygenases is primarily determined by the matchup between the substrate and binding pocket (28, 29). Numerous studies, typically involving sequences or structure alignment and site-directed mutagenesis, have demonstrated that such divergence is often caused by substitutions of several key residues, particularly those surrounding the active site (3, 15, 16, 18, 48, 63). An asparagine introduced at position 258 offers hydrogen bonding with nitroarene substrates, capturing and pinning the substrate in the active center and providing the preconditions for efficient denitration (3, 14–16, 21). Substitution of residues at positions 204, 293, and 350 would impact the activity and regiospecificity of nitrobenzene dioxygenase (3, 16, 18) and the well-studied naphthalene dioxygenase from *Pseudomonas* sp. NCIB 9816-4 (correspond to positions 206, 295, and 352 in $NDO_{9816\text{-}4}$) (71–73). Ju and Parales (17) and Mahan et al. (18) conducted long-term laboratory evolution experiments to generate mutants of 2-nitrotoluene dioxygenase from *Acidovorax* sp. strain JS42 that exhibited the ability to utilize 3- or 4-nitrotoluene. They found that residues outside the active site (238, 242, and 248 as reported by Ju and Parales and 405 according to Mahan et al.) could also modulate the catalytic activity, thereby offering a novel perspective for dioxygenase modification. The application of random mutagenesis (74) in the directed evolution of nitroarene dioxygenases has been limited in previous studies, primarily due to its potential to generate a vast library of mutants without efficient high-throughput screening methods.

This study introduces an *in silico* prediction approach for canonical site-directed mutagenesis to engineer 23DCNB dioxygenase with improved catalytic activity toward 24DCNB. The *in silico* results are basic anastomotic with the experimental findings, while the amount of time and labor involved in simulation is dramatically less than in the experiment. It is expected that this approach could be extended to other nitroarene dioxygenases for desired activity toward various nitroarenes. However, due to the limitation in our computing resources, we were only able to construct and evaluate a small mutant library. It is possible that other mutations, which we have not yet identified, also play a role in the transformation of this 23DCNB dioxygenase into a 24DCNB dioxygenase. Expanding the mutant library tested during the pre-screening phase may unveil additional advantageous mutations, thereby augmenting the catalytic activity of final mutant dioxygenase toward 24DCNB.

Our results bear out that the substituted positions of the substrate, rather than the types of its substituted groups, greatly influence the fitting process of nitroarene substrates in the active pocket of dioxygenase (28, 48). This feature further gives rise to the catalytic promiscuity of dioxygenases: as shown in the mutant dioxygenase substrate spectrum above (Fig. 4), the activity of a dioxygenase toward various nitroarene substrates is diverse, and mutations often result in the transfer of this activity to a class of substrates with similar substituted patterns.

The E204M mutation brought about a shift in preference of dioxygenase from *meta*- to *ortho*-substituted substrates, resulting from a more compact substrate pocket around the C3 atom of the substrate and thus a better fit for it. In general, the access through the enzyme channel and the orientation inside the active site of substrate both account for the catalytic efficiency, selectivity, and specificity (75–77). In view of the gatekeeper role of residue 204, it would be arbitrary to ignore any of the possible impact of residue 204 on the substrate as it passes through the enzyme tunnel or positioning in the active site. However, unlike $NDO_{9816\text{-}4}$, where an opening and obvious tunnel could be observed

from the protein surface (78), our wild-type or mutant dioxygenases have occluded tunnels, which could not be observed nor calculated. Our results highlighted residue 204 as a critical residue lining the catalytic cavity and supported a potential interaction between residue 204 and the *meta*-substituted group of nitroarenes (when it is properly bound to the active site) (18, 48).

The residue 248, although located outside the active site, has been identified as a crucial residue that potentially influences substrate specificity through its interaction with Asn295. Through this indirect effect, M248I mutation may exert some allosteric control on the active binding cavity around the C4 atom of the substrate, making it easier to accommodate *para*-substituted nitroarenes. Our findings corroborate the research carried out by Ju and Parales (17), in which long-term evolution provided 2-nitrotoluene dioxygenase with improved activity toward 4-nitrotoluene, and all three evolved mutants shared a common mutation—M248I.

Collectively, the coordinated interplay between E204M and M248I mutations retained the improved activity toward *ortho*- and *para*-substituted substrates, enhanced the catalytic activity toward 24DCNB, and thus the substrate spectrum was greatly broadened. E204M-M248I dioxygenase could be a versatile biocatalyst, supplying various nitroarene pollutants with hydroxyl groups for further transformation via ring cleavage and providing a new option for bioremediation in nitroarene-contaminated areas. The products transformed from 24DCNB were identified to be 35DCC, which can be completely mineralized through the degradation pathways discovered in *Cupriavidus necator* JMP134 (79–82), *Burkholderia cepacia* 2a (83), and *Cupriavidus gilardii* T-1 (84).

ACKNOWLEDGMENTS

This work was funded by the National Key R&D Program of China (2018YFA0901200 and 2021YFA0909500).

AUTHOR AFFILIATIONS

[1]State Key Laboratory of Microbial Metabolism, Joint International Research Laboratory of Metabolic and Developmental Sciences, School of Life Sciences and Biotechnology, Shanghai Jiao Tong University, Shanghai, China
[2]Department of Engineering Science, University of Oxford, Oxford, United Kingdom

AUTHOR ORCIDs

Jia Xu http://orcid.org/0009-0006-0797-8505
Tao Li http://orcid.org/0000-0002-8255-7798
Wei E. Huang http://orcid.org/0000-0003-1302-6528
Ning-Yi Zhou http://orcid.org/0000-0002-0917-5750

FUNDING

Funder	Grant(s)	Author(s)
MOST | National Key Research and Development Program of China (NKPs)	2018YFA0901200	Ning-Yi Zhou
MOST | National Key Research and Development Program of China (NKPs)	2021YFA0909500	Ning-Yi Zhou

DATA AVAILABILITY

The 2,3-dichloronitrobenzene dioxygenase (DcbAcAd) sequence of *Diaphorobacter* sp. strain JS3051 can be found under the GenBank accession numbers QPN31023.1 (DcbAc, α subunit) and QPN31022.1 (DcbAd, β subunit).

ADDITIONAL FILES

The following material is available online.

Supplemental Material

Supplemental figures (AEM01436-23-s0001.docx). Figures S1 to S7.

REFERENCES

1. Booth G. 2000. Nitro compounds, aromatic. In Ullmann's encyclopedia of industrial chemistry
2. Ju K-S, Parales RE. 2010. Nitroaromatic compounds, from synthesis to biodegradation. Microbiol Mol Biol Rev 74:250–272. https://doi.org/10.1128/MMBR.00006-10
3. Ju K-S, Parales RE. 2009. Application of nitroarene dioxygenases in the design of novel strains that degrade chloronitrobenzenes. Microb Biotechnol 2:241–252. https://doi.org/10.1111/j.1751-7915.2008.00083.x
4. Isayev O, Rasulev B, Gorb L, Leszczynski J. 2006. Structure-toxicity relationships of nitroaromatic compounds. Mol Divers 10:233–245. https://doi.org/10.1007/s11030-005-9002-4
5. Agency USEP. 2014. Priority pollutant list. Available from: https://www.epa.gov/sites/default/files/2015-09/documents/priority-pollutant-list-epa.pdf. Retrieved 8 Jul 2023.
6. Haigler BE, Wallace WH, Spain JC. 1994. Biodegradation of 2-nitrotoluene by *Pseudomonas* sp. strain JS42. Appl Environ Microbiol 60:3466–3469. https://doi.org/10.1128/aem.60.9.3466-3469.1994
7. Nishino SF, Spain JC. 1995. Oxidative pathway for the biodegradation of nitrobenzene by *Comamonas* sp. strain JS765. Appl Environ Microbiol 61:2308–2313. https://doi.org/10.1128/aem.61.6.2308-2313.1995
8. Singh D, Ramanathan G. 2013. Biomineralization of 3-nitrotoluene by *Diaphorobacter* species. Biodegradation 24:645–655. https://doi.org/10.1007/s10532-012-9612-3
9. Johnson GR, Jain RK, Spain JC. 2000. Properties of the trihydroxytoluene oxygenase from *Burkholderia cepacia* R34: an extradiol dioxygenase from the 2,4-dinitrotoluene pathway. Arch Microbiol 173:86–90. https://doi.org/10.1007/s002039900111
10. Johnson GR, Jain RK, Spain JC. 2002. Origins of the 2,4-dinitrotoluene pathway. J Bacteriol 184:4219–4232. https://doi.org/10.1128/JB.184.15.4219-4232.2002
11. Liu H, Wang S-J, Zhou N-Y. 2005. A new isolate of *Pseudomonas stutzerithat* degrades 2-chloronitrobenzene. Biotechnol Lett 27:275–278. https://doi.org/10.1007/s10529-004-8293-3
12. Palatucci ML, Waidner LA, Mack EE, Spain JC. 2019. Aerobic biodegradation of 2,3- and 3,4-dichloronitrobenzene. J Hazard Mater 378:120717. https://doi.org/10.1016/j.jhazmat.2019.05.110
13. Parales RE. 2003. The role of active-site residues in naphthalene dioxygenase. J Ind Microbiol Biotechnol 30:271–278. https://doi.org/10.1007/s10295-003-0043-3
14. Pabis A, Geronimo I, York DM, Paneth P. 2014. Molecular dynamics simulation of nitrobenzene dioxygenase using AMBER force field. J Chem Theory Comput 10:2246–2254. https://doi.org/10.1021/ct500205z
15. Lee K-S, Parales JV, Friemann R, Parales RE. 2005. Active site residues controlling substrate specificity in 2-nitrotoluene dioxygenase from *Acidovorax* sp. strain JS42. J Ind Microbiol Biotechnol 32:465–473. https://doi.org/10.1007/s10295-005-0021-z
16. Ju K-S, Parales RE. 2006. Control of substrate specificity by active-site residues in nitrobenzene dioxygenase. Appl Environ Microbiol 72:1817–1824. https://doi.org/10.1128/AEM.72.3.1817-1824.2006
17. Ju K-S, Parales RE. 2011. Evolution of a new bacterial pathway for 4-nitrotoluene degradation. Mol Microbiol 82:355–364. https://doi.org/10.1111/j.1365-2958.2011.07817.x
18. Mahan KM, Penrod JT, Ju K-S, Al Kass N, Tan WA, Truong R, Parales JV, Parales RE. 2015. Selection for growth on 3-nitrotoluene by 2-nitrotoluene-utilizing *Acidovorax* sp. strain JS42 identifies nitroarene dioxygenases with altered specificities. Appl Environ Microbiol 81:309–319. https://doi.org/10.1128/AEM.02772-14
19. Waterhouse AM, Procter JB, Martin DMA, Clamp M, Barton GJ. 2009. Jalview version 2--a multiple sequence alignment editor and analysis workbench. Bioinformatics 25:1189–1191. https://doi.org/10.1093/bioinformatics/btp033
20. Karlsson A, Parales JV, Parales RE, Gibson DT, Eklund H, Ramaswamy S. 2003. Crystal structure of naphthalene dioxygenase: side-on binding of dioxygen to iron. Science 299:1039–1042. https://doi.org/10.1126/science.1078020
21. Friemann R, Ivkovic-Jensen MM, Lessner DJ, Yu C-L, Gibson DT, Parales RE, Eklund H, Ramaswamy S. 2005. Structural insight into the dioxygenation of nitroarene compounds: the crystal structure of nitrobenzene dioxygenase. J Mol Biol 348:1139–1151. https://doi.org/10.1016/j.jmb.2005.03.052
22. Csizi KS, Eckert L, Brunken C, Hofstetter TB, Reiher M. 2022. The apparently unreactive substrate facilitates the electron transfer for dioxygen activation in rieske dioxygenases. Chem Eur J28:e202103937. https://doi.org/10.1002/chem.202103937
23. Wolfe MD, Parales JV, Gibson DT, Lipscomb JD. 2001. Single turnover chemistry and regulation of O_2 activation by the oxygenase component of naphthalene 1,2-dioxygenase. J Biol Chem 276:1945–1953. https://doi.org/10.1074/jbc.M007795200
24. Wolfe MD, Lipscomb JD. 2003. Hydrogen peroxide-coupled *cis*-diol formation catalyzed by naphthalene 1,2-dioxygenase. J Biol Chem 278:829–835. https://doi.org/10.1074/jbc.M209604200
25. Bassan A, Blomberg MRA, Siegbahn PEM. 2004. A theoretical study of the *cis*-dihydroxylation mechanism in naphthalene 1,2-dioxygenase. J Biol Inorg Chem 9:439–452. https://doi.org/10.1007/s00775-004-0537-0
26. Bassan A, Borowski T, Siegbahn PEM. 2004. Quantum chemical studies of dioxygen activation by mononuclear non-heme iron enzymes with the 2-His-1-carboxylate facial triad. Dalton Trans 20:3153–3162. https://doi.org/10.1039/B408340G
27. Sutherlin KD, Rivard BS, Böttger LH, Liu LV, Rogers MS, Srnec M, Park K, Yoda Y, Kitao S, Kobayashi Y, Saito M, Seto M, Hu M, Zhao J, Lipscomb JD, Solomon EI. 2018. NRVS studies of the peroxide shunt intermediate in a rieske dioxygenase and its relation to the native $Fe^{II}O_2$ reaction. J Am Chem Soc 140:5544–5559. https://doi.org/10.1021/jacs.8b01822
28. Bopp CE, Bernet NM, Kohler H-PE, Hofstetter TB. 2022. Elucidating the role of O_2 uncoupling in the oxidative biodegradation of organic contaminants by rieske non-heme iron dioxygenases. ACS Environ Au 2:428–440. https://doi.org/10.1021/acsenvironau.2c00023
29. Pati SG, Bopp CE, Kohler H-PE, Hofstetter TB. 2022. Substrate-specific coupling of O_2 activation to hydroxylations of aromatic compounds by rieske non-heme iron dioxygenases. ACS Catal 12:6444–6456. https://doi.org/10.1021/acscatal.2c00383
30. Agency USEP. The United States high production volume (USHPV) database. Available from: https://comptox.epa.gov/dashboard/chemical-lists/EPAHPV&search=DTXSID3024998 . Accessed July 8, 2023
31. Chen H, Gao X, Wang C, Shao J, Xu X, Zhu L. 2017. Efficient 2,4-dichloronitrobenzene removal in the coupled BES-UASB reactor: effect of external voltage mode. Bioresour Technol 241:879–886. https://doi.org/10.1016/j.biortech.2017.06.010
32. Chen L, Shao J, Chen H, Wang C, Gao X, Xu X, Zhu L. 2018. Cathode potential regulation in a coupled bioelectrode-anaerobic sludge system for effective dechlorination of 2,4-dichloronitrobenzene. Bioresour Technol 254:180–186. https://doi.org/10.1016/j.biortech.2018.01.092
33. Liu Y, Wang C, Zhang K, Zhou Y, Xu Y, Xu X, Zhu L. 2020. Rapid degradation of 2,4-dichloronitrobenzene in single-chamber microbial electrolysis cell with pre-acclimated bioanode: a comprehensive assessment. Sci Total Environ 724:138053. https://doi.org/10.1016/j.scitotenv.2020.138053
34. Kano H, Suzuki M, Senoh H, Yamazaki K, Aiso S, Matsumoto M, Nagano K, Fukushima S. 2012. 2,4-dichloro-1-nitrobenzene exerts carcinogenicities

in both rats and mice by two years feeding. Arch Toxicol 86:1763–1772. https://doi.org/10.1007/s00204-012-0890-7
35. Aleksic M, Pease CK, Basketter DA, Panico M, Morris HR, Dell A. 2008. Mass spectrometric identification of covalent adducts of the skin allergen 2,4-dinitro-1-chlorobenzene and model skin proteins. Toxicol In Vitro 22:1169–1176. https://doi.org/10.1016/j.tiv.2008.03.006
36. Agency USEP. International agency for research on cancer (IARC): group 2B: possibly carcinogenic to humans. Available from: https://comptox.epa.gov/dashboard/chemical-lists/IARC2B&search=DTXSID3024998. Accessed July 8, 2023
37. Jiang X, Shen J, Han Y, Lou S, Han W, Sun X, Li J, Mu Y, Wang L. 2016. Efficient nitro reduction and dechlorination of 2,4-dinitrochlorobenzene through the integration of bioelectrochemical system into upflow anaerobic sludge blanket: a comprehensive study. Water Res 88:257–265. https://doi.org/10.1016/j.watres.2015.10.023
38. Chen H, Lu D, Chen L, Wang C, Xu X, Zhu L. 2019. A study of the coupled bioelectrochemical system-upflow anaerobic sludge blanket for efficient transformation of 2,4-dichloronitrobenzene. Environ Sci Pollut Res 26:13002–13013. https://doi.org/10.1007/s11356-019-04751-9
39. Amrein BA, Steffen-Munsberg F, Szeler I, Purg M, Kulkarni Y, Kamerlin SCL. 2017. *CADEE*: computer-aided directed evolution of enzymes. IUCrJ 4:50–64. https://doi.org/10.1107/S2052252516018017
40. Wu L, Qin L, Nie Y, Xu Y, Zhao Y-L. 2022. Computer-aided understanding and engineering of enzymatic selectivity. Biotechnol Adv 54:107793. https://doi.org/10.1016/j.biotechadv.2021.107793
41. Go MK, Zhao LN, Xue B, Supekar S, Robinson RC, Fan H, Yew WS. 2020. Directed computational evolution of quorum-quenching lactonases from the amidohydrolase superfamily. Structure 28:635–642. https://doi.org/10.1016/j.str.2020.03.011
42. Waterhouse A, Bertoni M, Bienert S, Studer G, Tauriello G, Gumienny R, Heer FT, de Beer TAP, Rempfer C, Bordoli L, Lepore R, Schwede T. 2018. SWISS-MODEL: homology modelling of protein structures and complexes. Nucleic Acids Res 46:W296–W303. https://doi.org/10.1093/nar/gky427
43. Jumper J, Evans R, Pritzel A, Green T, Figurnov M, Ronneberger O, Tunyasuvunakool K, Bates R, Žídek A, Potapenko A, et al. 2021. Highly accurate protein structure prediction with AlphaFold. Nature 596:583–589. https://doi.org/10.1038/s41586-021-03819-2
44. Trott O, Olson AJ. 2010. AutoDock vina: improving the speed and accuracy of docking with a new scoring function, efficient optimization, and multithreading. J Comput Chem 31:455–461. https://doi.org/10.1002/jcc.21334
45. Vavra O, Filipovic J, Plhak J, Bednar D, Marques SM, Brezovsky J, Stourac J, Matyska L, Damborsky J. 2019. CaverDock: a molecular docking-based tool to analyse ligand transport through protein tunnels and channels. Bioinformatics 35:4986–4993. https://doi.org/10.1093/bioinformatics/btz386
46. Franz F, Daday C, Gräter F. 2020. Advances in molecular simulations of protein mechanical properties and function. Curr Opin Struct Biol 61:132–138. https://doi.org/10.1016/j.sbi.2019.12.015
47. Surpeta B, Sequeiros-Borja CE, Brezovsky J. 2020. Dynamics, a powerful component of current and future *in silico* approaches for protein design and engineering. Int J Mol Sci 21:2713. https://doi.org/10.3390/ijms21082713
48. Li T, Gao Y-Z, Xu J, Zhang S-T, Guo Y, Spain JC, Zhou N-Y. 2021. A recently assembled degradation pathway for 2,3-dichloronitrobenzene in *Diaphorobacter* sp. strain JS3051. mBio 12:e0223121. https://doi.org/10.1128/mBio.02231-21
49. An D, Gibson DT, Spain JC. 1994. Oxidative release of nitrite from 2-nitrotoluene by a three-component enzyme system from *Pseudomonas* sp. strain JS42. J Bacteriol 176:7462–7467. https://doi.org/10.1128/jb.176.24.7462-7467.1994
50. Bradford MM. 1976. A rapid and sensitive method for the quantitation of microgram quantities of protein utilizing the principle of protein-dye binding. Anal Biochem 72:248–254. https://doi.org/10.1006/abio.1976.9999
51. Anandakrishnan R, Aguilar B, Onufriev AV. 2012. H++ 3.0: automating pK prediction and the preparation of biomolecular structures for atomistic molecular modeling and simulations. Nucleic Acids Res 40:W537–41. https://doi.org/10.1093/nar/gks375
52. Li P, Merz KM. 2016. MCPB.py: a python based metal center parameter builder. J Chem Inf Model 56:599–604. https://doi.org/10.1021/acs.jcim.5b00674
53. Peters MB, Yang Y, Wang B, Füsti-Molnár L, Weaver MN, Merz KM. 2010. Structural survey of zinc-containing proteins and development of the zinc AMBER force field (ZAFF). J Chem Theory Comput 6:2935–2947. https://doi.org/10.1021/ct1002626
54. FrischMJ, TrucksGW, SchlegelHB, ScuseriaGE, RobbMA, CheesemanJR, Scalmani G, BaroneV, PeterssonGA, NakatsujiH, et al. 2016. Gaussian 16 Rev. C.01, Wallingford, CT
55. Gaussian. Inc. 2018 340 Quinnipiac street, building 40, Wallingford, CT 06392
56. Sousa da Silva AW, Vranken WF. 2012. ACPYPE - AnteChamber PYthon Parser interfacE. BMC Res Notes 5:367. https://doi.org/10.1186/1756-0500-5-367
57. Lindahl A, van der Spoel H. 2020. GROMACS 2020 source code (version 2020). https://doi.org/10.5281/zenodo.3562495
58. Hess B, Bekker H, Berendsen HJC, Fraaije JGEM. 1997. LINCS: a linear constraint solver for molecular simulations. J Comput Chem 18:1463–1472. https://doi.org/10.1002/(SICI)1096-987X(199709)18:12<1463::AID-JCC4>3.0.CO;2-H
59. Essmann U, Perera L, Berkowitz ML, Darden T, Lee H, Pedersen LG. 1995. A smooth particle mesh Ewald method. J Chem Phys 103:8577–8593. https://doi.org/10.1063/1.470117
60. Schrodinger LLC. 2015. The JyMOL molecular graphics development component, version 1.8
61. Wagner JR, Sørensen J, Hensley N, Wong C, Zhu C, Perison T, Amaro RE. 2017. POVME 3.0: software for mapping binding pocket flexibility. J Chem Theory Comput 13:4584–4592. https://doi.org/10.1021/acs.jctc.7b00500
62. Yu H, Ma S, Li Y, Dalby PA. 2022. Hot spots-making directed evolution easier. Biotechnol Adv 56:107926. https://doi.org/10.1016/j.biotechadv.2022.107926
63. Kumari A, Singh D, Ramaswamy S, Ramanathan G. 2017. Structural and functional studies of ferredoxin and oxygenase components of 3-nitrotoluene dioxygenase from *Diaphorobacter* sp. strain DS2. PLoS One 12:e0176398. https://doi.org/10.1371/journal.pone.0176398
64. Dannenberg JJ. 1998. An introduction to hydrogen bonding by George A. Jeffrey (University of Pittsburgh). J Am Chem Soc 120:5604–5604. https://doi.org/10.1021/ja9756331
65. Starr TN, Thornton JW. 2016. Epistasis in protein evolution. Protein Sci. 25:1204–1218. https://doi.org/10.1002/pro.2897
66. Wang Z, Zhou H, Yu H, Pu Z, Xu J, Zhang H, Wu J, Yang L. 2022. Computational redesign of the substrate binding pocket of glutamate dehydrogenase for efficient synthesis of noncanonical L-amino acids . ACS Catal 12:13619–13629. https://doi.org/10.1021/acscatal.2c04636
67. Yu H, Dalby PA. 2018. Coupled molecular dynamics mediate long- and short-range epistasis between mutations that affect stability and aggregation kinetics. Proc Natl Acad Sci U S A 115:E11043–E11052. https://doi.org/10.1073/pnas.1810324115
68. Liu H, Wang S-J, Zhang J-J, Dai H, Tang H, Zhou N-Y. 2011. Patchwork assembly of nag-like nitroarene dioxygenase genes and the 3-chlorocatechol degradation cluster for evolution of the 2-chloronitrobenzene catabolism pathway in *Pseudomonas stutzeri* ZWLR2-1. Appl Environ Microbiol 77:4547–4552. https://doi.org/10.1128/AEM.02543-10
69. Gao Y-Z, Liu X-Y, Liu H, Guo Y, Zhou N-Y. 2020. A Bph-like nitroarene dioxygenase catalyzes the conversion of 3-nitrotoluene to 3-methylcatechol by *Rhodococcus* sp. strain ZWL3NT. Appl Environ Microbiol 86:e02517-19. https://doi.org/10.1128/AEM.02517-19
70. Li T, Xu J, Brower AL, Xu Z-J, Xu Y, Spain JC, Zhou N-Y. 2023. Molecular basis and evolutionary origin of 1-nitronaphthalene catabolism in *Sphingobium* sp. strain JS3065. Appl Environ Microbiol 89:e0172822. https://doi.org/10.1128/aem.01728-22
71. Yu CL, Parales RE, Gibson DT. 2001. Multiple mutations at the active site of naphthalene dioxygenase affect regioselectivity and enantioselectivity. J Ind Microbiol Biotechnol 27:94–103. https://doi.org/10.1038/sj.jim.7000168
72. Parales RE, Resnick SM, Yu CL, Boyd DR, Sharma ND, Gibson DT. 2000. Regioselectivity and enantioselectivity of naphthalene dioxygenase during arene *cis*-dihydroxylation: control by phenylalanine 352 in the α

subunit. J Bacteriol 182:5495–5504. https://doi.org/10.1128/JB.182.19.5495-5504.2000
73. Seo J, Ryu JY, Han J, Ahn JH, Sadowsky MJ, Hur HG, Chong Y. 2013. Amino acid substitutions in naphthalene dioxygenase from *Pseudomonas* sp. strain NCIB 9816-4 result in regio- and stereo-specific hydroxylation of flavanone and isoflavanone. Appl Microbiol Biotechnol 97:693–704. https://doi.org/10.1007/s00253-012-3962-y
74. Bernath-Levin K, Shainsky J, Sigawi L, Fishman A. 2014. Directed evolution of nitrobenzene dioxygenase for the synthesis of the antioxidant hydroxytyrosol. Appl Microbiol Biotechnol 98:4975–4985. https://doi.org/10.1007/s00253-013-5505-6
75. Kreß N, Halder JM, Rapp LR, Hauer B. 2018. Unlocked potential of dynamic elements in protein structures: channels and loops. Curr Opin Chem Biol 47:109–116. https://doi.org/10.1016/j.cbpa.2018.09.010
76. Kokkonen P, Bednar D, Pinto G, Prokop Z, Damborsky J. 2019. Engineering enzyme access tunnels. Biotechnol Adv 37:107386. https://doi.org/10.1016/j.biotechadv.2019.04.008
77. Liu J, Tian J, Perry C, Lukowski AL, Doukov TI, Narayan ARH, Bridwell-Rabb J. 2022. Design principles for site-selective hydroxylation by a Rieske oxygenase. Nat Commun 13:255. https://doi.org/10.1038/s41467-021-27822-3
78. Escalante DE, Aukema KG, Wackett LP, Aksan A. 2017. Simulation of the bottleneck controlling access into a rieske active site: predicting substrates of naphthalene 1,2-dioxygenase. J Chem Inf Model 57:550–561. https://doi.org/10.1021/acs.jcim.6b00469
79. Kumar A, Trefault N, Olaniran AO. 2016. Microbial degradation of 2,4-dichlorophenoxyacetic acid: insight into the enzymes and catabolic genes involved, their regulation and biotechnological implications. Crit Rev Microbiol 42:194–208. https://doi.org/10.3109/1040841X.2014.917068
80. Pérez-Pantoja D, Ledger T, Pieper DH, González B. 2003. Efficient turnover of chlorocatechols is essential for growth of *Ralstonia eutropha* JMP134(pJP4) in 3-chlorobenzoic acid. J Bacteriol 185:1534–1542. https://doi.org/10.1128/JB.185.5.1534-1542.2003
81. Plumeier I, Pérez-Pantoja D, Heim S, González B, Pieper DH. 2002. Importance of different *tfd* genes for degradation of chloroaromatics by *Ralstonia eutropha* JMP134. J Bacteriol 184:4054–4064. https://doi.org/10.1128/JB.184.15.4054-4064.2002
82. Pérez-Pantoja D, Guzmán L, Manzano M, Pieper DH, González B. 2000. Role of $tfdC_ID_IE_IF_I$ and $tfdD_{II}C_{II}E_{II}F_{II}$ gene modules in catabolism of 3-chlorobenzoate by *Ralstonia eutropha* JMP134(pJP4). Appl Environ Microbiol 66:1602–1608. https://doi.org/10.1128/AEM.66.4.1602-1608.2000
83. Smith ARW, Beadle CA. 2008. Induction of enzymes of 2,4-dichlorophenoxyacetate degradation in *Burkholderia cepacia* 2A and toxicity of metabolic intermediates. Biodegradation 19:669–681. https://doi.org/10.1007/s10532-007-9172-0
84. Wu X, Wang W, Liu J, Pan D, Tu X, Lv P, Wang Y, Cao H, Wang Y, Hua R. 2017. Rapid biodegradation of the herbicide 2,4-dichlorophenoxyacetic acid by *Cupriavidus Gilardii* T-1. J Agric Food Chem 65:3711–3720. https://doi.org/10.1021/acs.jafc.7b00544